DSP Implementation of an Active Bearing Mount for Rotors Using Hybrid Control

Mingsian R. Bai

Weibin Luo

Department of Mechanical Engineering,
National Chiao-Tung University,
1001 Ta-Hsueh Road,
Hsin-Chu, Taiwan, Republic of China

An on-line active technique for suppressing rotor vibration is proposed. Electromagnetic actuators are mounted on the housing of a ball bearing for generating counter forces to cancel the transverse vibrations due to imbalance, misalignment, and so forth. Controllers based on feedback structure, feedforward structure and hybrid structure are investigated. The multiple channel active control systems are implemented on the platform of a digital signal processor. Numerical simulation and experimental investigations indicate that the proposed methods are effective in suppressing the periodic disturbances. In particular, the hybrid control by using feedback linear quadratic gaussian control and feedforward least mean square algorithm with synthetic reference achieves the best performance in terms of vibration attenuation and convergence speed.
[S0739-3717(00)00904-1]

1 Introduction

Common causes of vibration in rotating machinery are imbalance, misalignment, looseness, and so forth. These rotor faults may results in excessive vibration amplitude in the fundamental frequency as well as its multiples which will in turn produce adverse effects on noise, reliability and performance of machines. For example, in precision machining using a high-speed lathe, excessive transverse vibration of the spindle may result in unacceptable errors and even the failure of the machine tool. Conventional ways of reducing the vibration due to imbalance and misalignment are to apply standard procedures to align and dynamically balance the machine of interest in an off-line fashion. In this paper, an on-line and real-time active technique for suppressing rotor vibration is proposed. Electro-magnetic actuators are mounted on the housing of a ball bearing to generate the required counter forces.

There have been many studies devoted to the subject of active control of rotors. Based on flight attitude formulation, Matsumura and Yoshimoto [1] derived an analytical model for active control technique using magnetic bearings. Börvik and Högfors [2] derived an equation of motion for a disc using two-mass autobalancer. On the basis of Börvik and Högfors' formulation, Lum et al. [3,4] developed an iterative method to control rotor vibration due to imbalance. Among the researchers in this area, Palazzolo and his coworkers have made remarkable contribution in a series of papers. Palazzolo et al. [5] proposed an active method using linear quadratic optimization to control the transient vibration of rotor. Palazzolo et al. [6,7] also developed an active control system using ''piezoelectric pushers'' for suppressing steady state as well as transient state of rotor vibration. In contrast to the contact type of actuator used by Palazzolo et al., Knospe et al. [8] proposed an iterative scheme to compensate imbalance vibration in active magnetic bearings (AMB) systems. A very good review of the research on AMB can be found in the paper by Bleuler [9].

Instead of using costly AMB systems, the active technique presented in this paper is targeted at the transverse vibration in the housing of ball bearings which remain the key components in industrial applications. The control system includes two electromagnetic actuators, two eddy current sensors, a photo switch and a digital signal processor (DSP)-based controller. Because of gyroscopic effects, the system dynamics are coupled in proportion to rotating speed and thus multiple channel control is employed to deal with this problem. Controllers based on feedback structure, feedforward structure and hybrid structure are compared. Numerical simulation and experimental investigations indicate that the proposed methods are effective in suppressing the transverse vibrations in both horizontal and vertical directions to the shaft. In particular, the hybrid control by using linear quadratic gaussian (LQG) control in the feedback compensator and adaptive least mean square (LMS) algorithm with synthetic reference in the feedforward controller achieves the best performance in terms of vibration attenuation and convergence speed. Design considerations during implementation phase and future research aspects are also addressed in the paper.

2 Modeling of Rotor Dynamics

It can be shown by energy method that the nonplanar motion of a rigid rotor is expressed as [10,11]

$$\begin{bmatrix} M & 0 & 0 & 0 \\ 0 & M & 0 & 0 \\ 0 & 0 & I_t & 0 \\ 0 & 0 & 0 & I_t \end{bmatrix} \begin{bmatrix} \ddot{R}_X \\ \ddot{R}_Y \\ \ddot{\beta}_Y \\ \ddot{\beta}_X \end{bmatrix} + \dot{\varphi} \begin{bmatrix} 0 & 0 & 0 & 0 \\ 0 & 0 & 0 & 0 \\ 0 & 0 & 0 & -I_p \\ 0 & 0 & I_p & 0 \end{bmatrix} \begin{bmatrix} \dot{R}_X \\ \dot{R}_Y \\ \dot{\beta}_Y \\ \dot{\beta}_X \end{bmatrix}$$

Contributed by the Technical Committee on Vibration and Sound for publication in the JOURNAL OF VIBRATION AND ACOUSTICS. Manuscript received July 1999; revised April 2000. Associate Technical Editor: J. Q. San.

$$+\begin{bmatrix} C_{X1}+C_{X2} & 0 & \ell_2 C_{X2}-\ell_1 C_{X1} & 0 \\ 0 & C_{Y1}+C_{Y2} & 0 & \ell_1 C_{Y1}-\ell_2 C_{Y2} \\ \ell_2 C_{X2}-\ell_1 C_{X1} & 0 & \ell_1^2 C_{Y1}+\ell_2^2 C_{Y2} & 0 \\ 0 & \ell_2 C_{X2}-\ell_1 C_{X1} & 0 & \ell_1^2 C_{X1}+\ell_2^2 C_{X2} \end{bmatrix}\begin{bmatrix} \dot{R}_X \\ \dot{R}_Y \\ \dot{\beta}_Y \\ \dot{\beta}_X \end{bmatrix}$$

$$+\begin{bmatrix} k_{X1}+k_{X2} & 0 & \ell_2 k_{X2}-\ell_1 k_{X1} & 0 \\ 0 & k_{Y1}+k_{Y2} & 0 & \ell_1 k_{Y1}-\ell_2 k_{Y2} \\ \ell_2 k_{X2}-\ell_1 k_{X1} & 0 & \ell_1^2 k_{Y1}+\ell_2^2 k_{Y2} & 0 \\ 0 & \ell_2 k_{X2}-\ell_1 k_{X1} & 0 & \ell_1^2 k_{X1}+\ell_2^2 k_{X2} \end{bmatrix}\begin{bmatrix} R_X \\ R_Y \\ \beta_Y \\ \beta_X \end{bmatrix} = \dot{\varphi}^2 \begin{bmatrix} m_u a_X \\ m_u a_Y \\ 0 \\ 0 \end{bmatrix} \tag{1}$$

where M is the mass of rotor, I_p is the polar moment of inertia, I_t is the transverse moment of inertia, m_u is the imbalance mass, (a_X, a_Y) is the location of the imbalance, R_X and R_Y are the displacements in X and Y directions, β_X and β_Y are the Euler's angles in X and Y directions, C_{pn} and k_{pn} ($p=X,Y$; $n=1,2$ of the bearing number) are damping and stiffness coefficients, ℓ_1 and ℓ_2 are the distances between two bearings to the disk, and $\dot{\varphi}$ is the rotating speed of the shaft. It is noted in Eq. (1) that the second coefficient matrix is skew-symmetric and thus energy lossless. This term representing the gyroscopic effect in proportion to the rotating speed results in the coupling between the dynamics of two axes.

In order for the subsequent use of active control, the equation of motion of Eq. (1) is converted into the following state-space form:

$$\dot{\mathbf{x}} = \mathbf{A}\mathbf{x} + \mathbf{B}\mathbf{u}$$

$$\mathbf{y} = \mathbf{C}\mathbf{x} + \mathbf{D}\mathbf{u}, \tag{2}$$

where

$$\mathbf{x} = \begin{Bmatrix} x_1 \\ x_2 \\ x_3 \\ x_4 \\ x_5 \\ x_6 \\ x_7 \\ x_8 \end{Bmatrix} = \begin{Bmatrix} R_X \\ \dot{R}_X \\ \beta_Y \\ \dot{\beta}_Y \\ R_Y \\ \dot{R}_Y \\ \beta_X \\ \dot{\beta}_X \end{Bmatrix}$$

is the state vector,

$$\mathbf{u} = \begin{bmatrix} em_u & \cos\dot{\varphi}t \\ em_u & \sin\dot{\varphi}t \end{bmatrix}$$

is the input vector,

$$\mathbf{y} = \begin{bmatrix} R_X \\ R_Y \end{bmatrix}$$

is the output vector,

$$\mathbf{A} = \begin{bmatrix} \mathbf{A}_{11} & \mathbf{A}_{12} \\ \mathbf{A}_{21} & \mathbf{A}_{22} \end{bmatrix},$$

$$\mathbf{A}_{11} = \begin{bmatrix} 0 & 1 & 0 & 0 \\ \dfrac{-(K_{X1}+K_{X2})}{M} & \dfrac{-(C_{X1}+C_{X2})}{M} & \dfrac{\ell_1 K_{X1}-\ell_2 K_{X2}}{M} & \dfrac{\ell_1 C_{X1}-\ell_2 C_{X2}}{M} \\ 0 & 0 & 0 & 1 \\ \dfrac{\ell_1 K_{X1}-\ell_2 K_{X2}}{I_t} & \dfrac{\ell_1 C_{X1}-\ell_2 C_{X2}}{I_t} & \dfrac{-(\ell_1^2 K_{X1}+\ell_2^2 K_{X2})}{I_t} & \dfrac{-(\ell_1^2 C_{X1}+\ell_2^2 C_{X2})}{I_t} \end{bmatrix}, \quad \mathbf{A}_{12} = \begin{bmatrix} 0 & 0 & 0 & 0 \\ 0 & 0 & 0 & 0 \\ 0 & 0 & 0 & 0 \\ 0 & 0 & 0 & \dfrac{\dot{\varphi} I_p}{I_t} \end{bmatrix},$$

$$\mathbf{A}_{21} = \begin{bmatrix} 0 & 0 & 0 & 0 \\ 0 & 0 & 0 & 0 \\ 0 & 0 & 0 & 0 \\ 0 & 0 & 0 & \dfrac{-\dot{\varphi} I_p}{I_t} \end{bmatrix}, \quad \mathbf{A}_{22} = \begin{bmatrix} 0 & 1 & 0 & 0 \\ \dfrac{-(K_{Y1}+K_{Y2})}{M} & \dfrac{-(C_{Y1}+C_{Y2})}{M} & \dfrac{\ell_2 K_{Y2}-\ell_1 K_{Y1}}{M} & \dfrac{\ell_2 C_{Y2}-\ell_1 C_{Y1}}{M} \\ 0 & 0 & 0 & 1 \\ \dfrac{\ell_2 K_{Y2}-\ell_1 K_{Y1}}{I_t} & \dfrac{\ell_2 C_{Y2}-\ell_1 C_{Y1}}{I_t} & \dfrac{-(\ell_1^2 K_{Y1}+\ell_2^2 K_{Y2})}{I_t} & \dfrac{-(\ell_1^2 C_{Y1}+\ell_2^2 C_{Y2})}{I_t} \end{bmatrix},$$

$$\mathbf{B}=\begin{bmatrix} 0 & 0 \\ \dfrac{\bar{\varphi}^2\cos\varphi_0}{M} & \dfrac{-\bar{\varphi}^2\sin\varphi_0}{M} \\ 0 & 0 \\ 0 & 0 \\ 0 & 0 \\ \dfrac{\bar{\varphi}^2\sin\varphi_0}{M} & \dfrac{\bar{\varphi}^2\cos\varphi_0}{M} \\ 0 & 0 \\ 0 & 0 \end{bmatrix}, \qquad \mathbf{C}=\begin{bmatrix} 1 & 0 & 0 & 0 & 0 & 0 & 0 & 0 \\ 0 & 0 & 0 & 0 & 1 & 0 & 0 & 0 \end{bmatrix}.$$

3 Active Vibration Control of Rotors

There are in general two strategies for active control of rotors: imbalance compensation and autocentering [12]. The former approach is to align the geometric axis with the rotating axis such that the transverse displacements of the shaft are minimal. However, the reaction forces at the bearing could be large in this case. Conversely, the latter approach is to align the principal inertia axis with the rotating axis such that the reaction forces at the bearing are minimal. However, the transverse displacements of the shaft could be large in this case. This paper adopted the first approach because of the potential application of the system to precision machining.

This paper is focused on the development of online and real-time active control techniques for rotor vibrations. The control structures used in controller synthesis are feedback, feedforward and hybrid structures [13]. Feedback structure requires a sensor that generally plays a dual role as a measurement sensor and as a performance sensor. Performance and stability should be carefully compromised, especially in the presence of system uncertainties and perturbations. Using feedback structure, performance can usually be achieved at only narrow bands. Unlike feedback structure, feedforward structure has no stability problem and broadband performance is generally possible. However, the performance of feedforward control is not robust in comparison with feedback structure. Hybrid control combines the merits of both structures: robustness is improved by feedback control and broadband performance is achieved by feedforward control. In addition, the convergence speed of the LMS algorithm can be significantly increased in using hybrid structure, as will become clear later. The design strategy of hybrid control is first to find a feedback compensator that stabilizes the open-loop system, and then introduce a feedforward controller to achieve performance without degrading the stability of the feedback-compensated system. This sequential design procedure of the hybrid structure has been justified by a separation principle, as detailed in the paper by Clark and Bernstein [14].

3.1 Feedback Structure: LQG Synthesis and Internal Model Principle. Feedback structure has been the main stream of control system design. In this paper, LQG synthesis is employed in the design of the feedback controller. LQG design involves a state feedback module and a Kalman-Bucy observer [15,16]. The former corresponds to the following control law:

$$\mathbf{u}(k)=-\mathbf{K}\mathbf{x}(k), \tag{3}$$

where **K** denotes the state feedback gain. To determine **K**, the following linear quadratic performance index is minimized such that the control error and the control effort are reasonably balanced:

$$J=E\left\{\sum_{k=1}^{\infty}\left[\mathbf{x}^T(k)\mathbf{Q}_c\mathbf{x}(k)+\mathbf{u}^T(k)\mathbf{R}_c\mathbf{u}(k)\right]\right\}, \tag{4}$$

where $\mathbf{Q}_c$ is a positive semi-definite matrix and $\mathbf{R}_c$ is a positive definite matrix. In the paper, we choose

$$\mathbf{Q}_c=q_cI, \tag{5}$$

and

$$\mathbf{R}_c=r_cI, \tag{6}$$

where $q_c\geqslant 0$, $r_c>0$ are two scalar constants, **I**'s are identity matrices with matched dimensions. The optimal gain vector is

$$\mathbf{K}=(\mathbf{R}_c+\mathbf{B}^T\mathbf{P}\mathbf{B})^{-1}\mathbf{B}^T\mathbf{P}\mathbf{A}, \tag{7}$$

where the positive definite matrix **P** is the solution of the following algebraic Riccati equation

$$\mathbf{A}^T\mathbf{P}\mathbf{A}-\mathbf{P}-\mathbf{A}^T\mathbf{P}\mathbf{B}(\mathbf{R}_c+\mathbf{B}^T\mathbf{P}\mathbf{B})^{-1}\mathbf{B}^T\mathbf{P}\mathbf{A}+\mathbf{Q}_c=\mathbf{0}. \tag{8}$$

In practice, it may not be possible to measure all state variables. This calls for the need of a Kalman filter-based state observer

$$\hat{\mathbf{x}}(k+1)=\mathbf{A}\hat{\mathbf{x}}(k)+\mathbf{B}\mathbf{u}(k)+\mathbf{L}[\mathbf{y}(k)-\mathbf{C}\hat{\mathbf{x}}(k)-\mathbf{D}\mathbf{u}(k)]. \tag{9}$$

In this equation, $\hat{\mathbf{x}}$ denotes the estimated state and the observer gain is obtained from

$$\mathbf{L}=\mathbf{A}\mathbf{P}\mathbf{C}^T(\mathbf{C}\mathbf{P}\mathbf{C}^T+\mathbf{R}_f)^{-1}, \tag{10}$$

where the positive definite matrix **P** satisfies the following algebraic Riccati equation

$$\mathbf{A}\mathbf{P}\mathbf{A}^T+\mathbf{G}\mathbf{Q}_f\mathbf{G}^T-\mathbf{P}-\mathbf{A}\mathbf{P}\mathbf{C}^T(\mathbf{C}\mathbf{P}\mathbf{C}^T+\mathbf{R}_f)^{-1}\mathbf{C}\mathbf{P}\mathbf{A}^T=\mathbf{0}. \tag{11}$$

The weighting matrices **Q** and **R** are of the similar form as the state feedback of Eqs. (4) and (5). One of the advantages of using

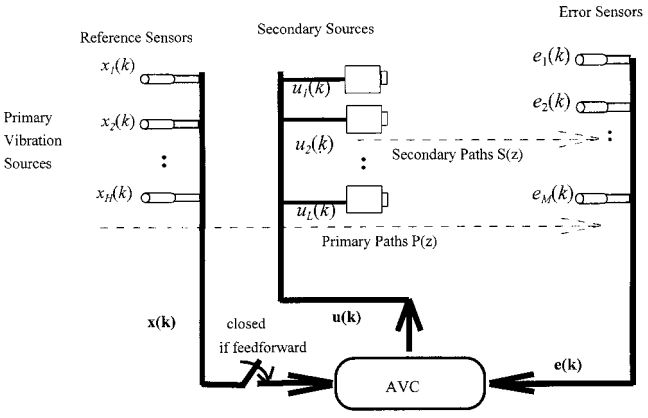

Fig. 1 MIMO active vibration control system

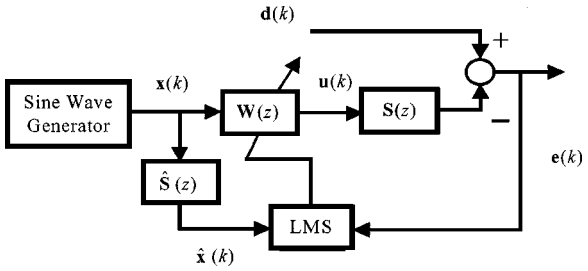

Fig. 2 Feedforward FXLMS algorithm with synthetic reference

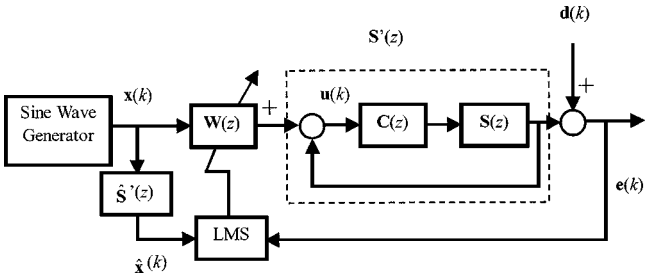

Fig. 3 Hybrid structure with feedback LQG control and feedforward FXLMS control

LQG technique lies in the *separation principle* [16], which simply states that the design of state feedback and state observer can be carried out separately.

For high order systems, it is generally difficult to achieve broadband attenuation using collocated feedback structure. This is an inherent drawback of the feedback structure due to the classical *Bode's integral constraint* [13]. Therefore, we chose to use a less demanding approach based on *the internal model principle* [17] so that the performance at some spectral peaks can be achieved. This requires inserting a disturbance model into the feedback loop to create a large gain at certain frequencies.

For a periodic noise of m frequency components, the discrete-time internal model can be chosen as the following form:

$$D(z)=\sum_{n=1}^{m}\frac{T}{\omega_n}\frac{-M_n r_n \sin(\omega_n T)z^{-1}}{1-2r_n\cos(\omega_n T)z^{-1}+r_n^2 z^{-2}}, \qquad (12)$$

where T is the sampling period, ω_n, $n=1,2,\ldots,m$ are the peak frequencies, $r_n=e^{-\zeta_n\omega_n T}$, ζ_n is the damping ratio, and M_n is the gain. The choice of ζ_n depends on how one weights the maximal attenuation and the bandwidth of attenuation, within the limit of stability. Note that $D(z)$ is essentially a superposition of second-order systems. It produces very large gains at the pre-specified frequencies ω_n that can be obtained by some means, e.g., a tachometer. To incorporate the disturbance model into the MIMO system, we augment the model into a diagonal transfer matrix

$$\mathbf{D}(z)=D(z)\mathbf{I}_{r\times r}, \qquad (13)$$

where $\mathbf{I}_{r\times r}$ is an identity matrix and r is the number of inputs. The design procedure is first to include $\mathbf{D}(z)$ as part of the plant and then find a compensator $\mathbf{C}(z)$ to stabilize the closed-loop system by LQG synthesis. The resulting controller to implement is simply the cascaded transfer function $\mathbf{C}(z)\mathbf{D}(z)$.

3.2 Feedforward Structure: MIMO FXLMS Algorithm With Synthetic Reference. As an alternative to feedback structure, feedforward structure is also employed in the research. The MIMO filtered-x least mean square (FXLMS) algorithm with synthetic reference [18] is utilized in this control structure. In the active control system depicted in Fig. 1, H reference signals, $x_h(k)$, are measured by H reference sensors. The control signals

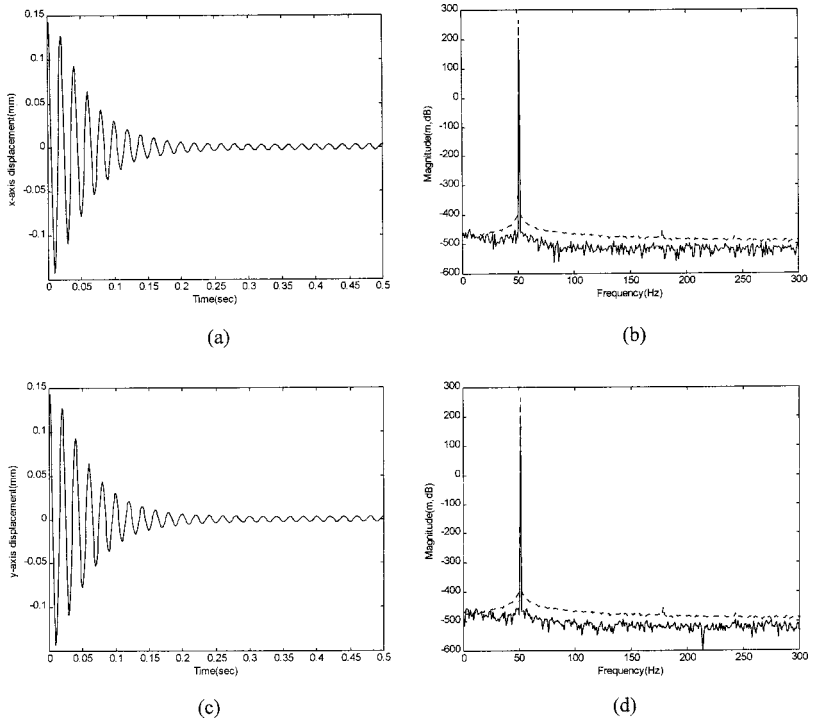

Fig. 4 Simulation results of feedback LQG control. (*a*) *X*-axis time signal of residual vibration after control (transient response); (*b*) *X*-axis steady-state power spectra of vibration (. . . control off,_control on); (*c*) *Y*-axis time signal of residual vibration after control (transient response); (*d*) *Y*-axis steady-state power spectra of vibration (. . . control off,_control on).

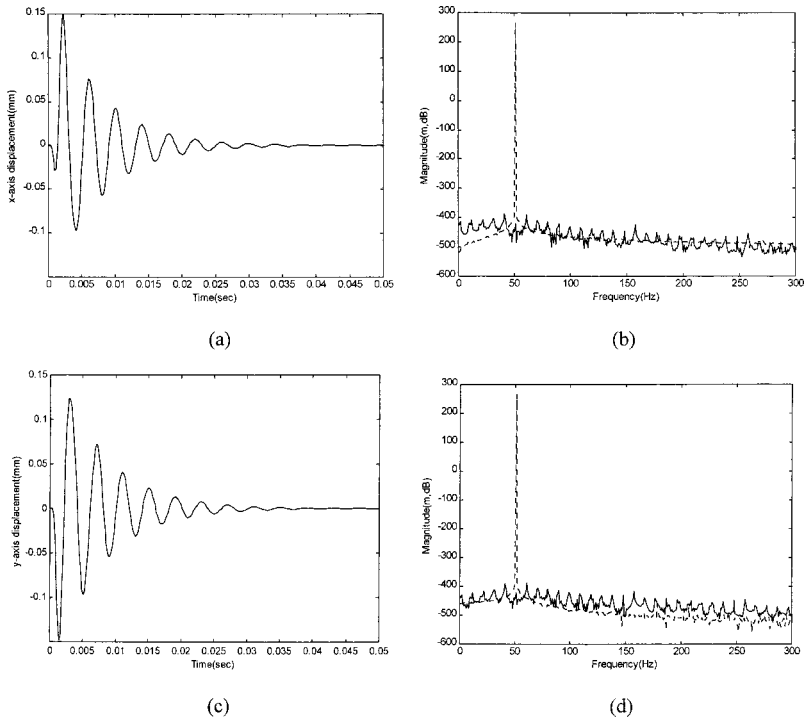

Fig. 5 Simulation results of feedforward FXLMS control with synthetic reference. (*a*) *X*-axis time signal of residual vibration after control (transient response); (*b*) *X*-axis steady-state power spectra of vibration (. . . control off,_ control on); (*c*) *Y*-axis time signal of residual vibration after control (transient response); (*d*) *Y*-axis steady-state power spectra of vibration (. . . control off,_control on).

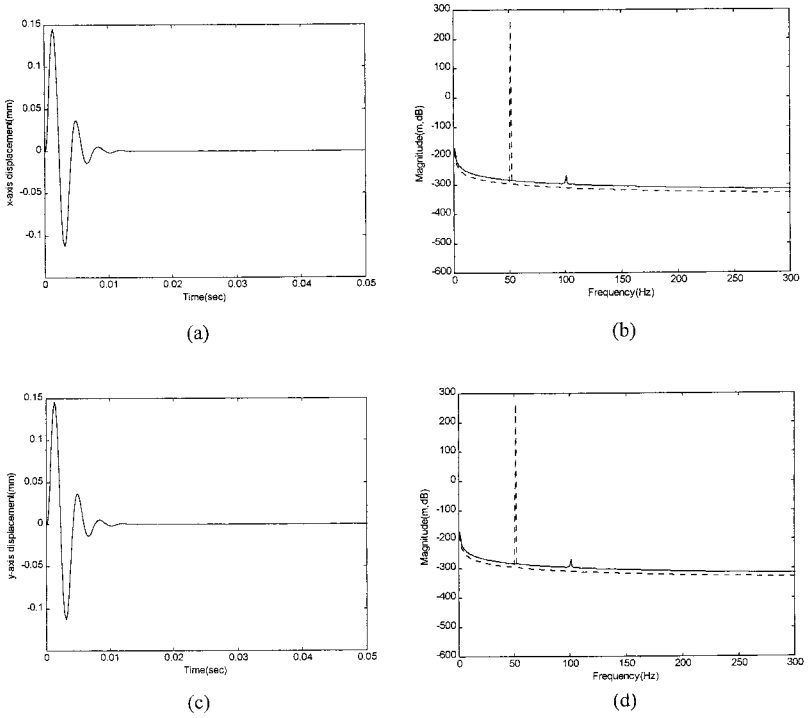

Fig. 6 Simulation results of hybrid control. (*a*) *X*-axis time signal of residual vibration after control (transient response); (*b*) *X*-axis steady-state power spectra of vibration (. . . control off,_control on); (*c*) *Y*-axis time signal of residual vibration after control (transient response); (*d*) *Y*-axis steady-state power spectra of vibration (. . . control off,_control on).

$u_l(k)$ driving the L secondary sources are produced by the MIMO controller that in turn comprised of $L \times H$ I-th order FIR filters with coefficients, w_{lhi}. Then the control signals from the controller can be written as

$$u_l(k) = \sum_{h=1}^{H} \sum_{i=0}^{I-1} w_{lhi} x_h(k-i). \tag{14}$$

The secondary paths are modeled as J-th order FIR filters with coefficients, s_{mlj}. The error signal measured by the m-th error sensor can be expressed as

$$e_m(k) = d_m(k) + \sum_{l=1}^{L} \sum_{j=0}^{J-1} s_{mlj} u_l(k-j), \tag{15}$$

where $d_m(k)$ is the primary noise measured at the m-th error sensor. By the gradient search that seeks to minimize the cost function

$$J(k) = \sum_{m=1}^{M} e_m^2(k), \tag{16}$$

one can obtain the update formula of the filter coefficients

$$w_{lhi}(k+1) = w_{lhi}(k) - \mu \sum_{m=1}^{M} e_m r_{mlh}(k-i), \tag{17}$$

where μ is the step size (or convergence factor) and r_{mlj} is

$$r_{mlj}(k) = \sum_{j=0}^{J-1} \hat{s}_{mlj} x_h(k-j). \tag{18}$$

The block diagram of the MIMO FXLMS algorithm is given in Fig. 2, where $\mathbf{u}(k)$ is the control signal, $\mathbf{W}(z)$ is the transfer matrix of the FIR filter, $\mathbf{d}(k)$ is the primary noise, $\mathbf{e}(k)$ is the error signal, and the matrix $\hat{\mathbf{S}}(z)$ represents the estimated secondary path $\mathbf{S}(z)$.

Since rotor vibration *per se* generally contains tones at the fundamental frequency and its multiples, we use a synthetic scheme to generate a reference for the FXLMS algorithm. The main benefit of this approach is that undesired positive feedback problem is virtually eliminated. In Fig. 2, a sine wave generator based on a marginally stable two-pole resonator is employed to generate synthetic signals $\mathbf{x}(k)$ with prescribed frequency [18]. The transfer function of the generator is

$$H(z) = \frac{\sin(\omega_n T) z^{-1}}{1 - 2\cos(\omega_n T) z^{-1} + z^{-2}}, \tag{19}$$

where T is the sampling period and ω_n is the prescribed frequency of the sinusoid. This second-order IIR filter corresponds to the following difference equation

$$y(k) = 2\cos(\omega_n T) y(k-1) - y(k-2), \tag{20}$$

with initial conditions

$$y(1) = A \sin(\omega_n T), \tag{21}$$

and

$$y(0) = 0, \tag{22}$$

where A is the amplitude of the desired sinusoid. Similarly, if there are more than one frequency component in the disturbance, one simply adds more terms to the sine wave generators. The phasing of the generator is not important.

3.3 Hybrid Structure: Feedforward FXLMS and Feedback LQG Algorithm. To further enhance the active control system, a hybrid structure is exploited by combining the aforementioned feedforward control and feedback control. The block diagram is shown in Fig. 3, where $\mathbf{u}(k)$ is the control signal, $\mathbf{W}(z)$ is the transfer matrix of the FIR filter, $\mathbf{d}(k)$ is the primary noise, $\mathbf{e}(k)$ is the error signal, and

Table 1 Summary of numerical simulation

	Axis	Attenuation (dB)	Convergence Speed (sec)
Feedback LQG with internal model	x-axis and y-axis	85	0.3
Feedforward FXLMS	x-axis and y-axis	680	0.04
Hybrid FXLMS with LQG	y-axis and x-axis	550	0.01

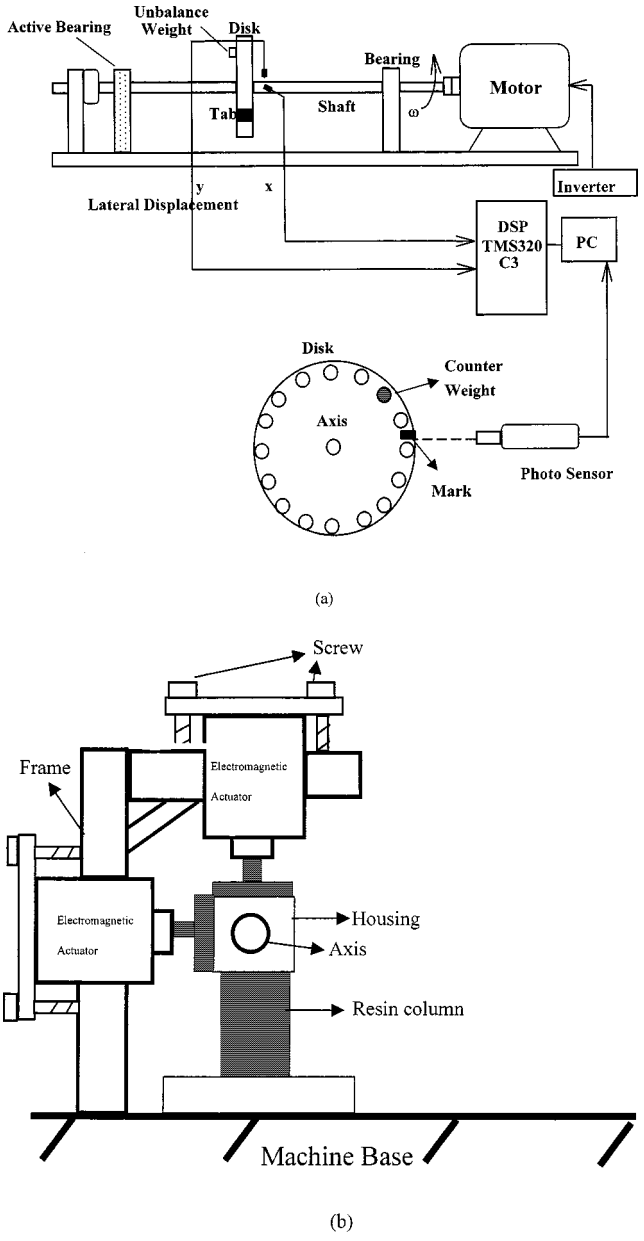

Fig. 7 Experimental arrangement of the active rotor vibration control system. (*a*) Schematic of experimental setup; (*b*) close-up of the mounting of electro-magnetic actuators.

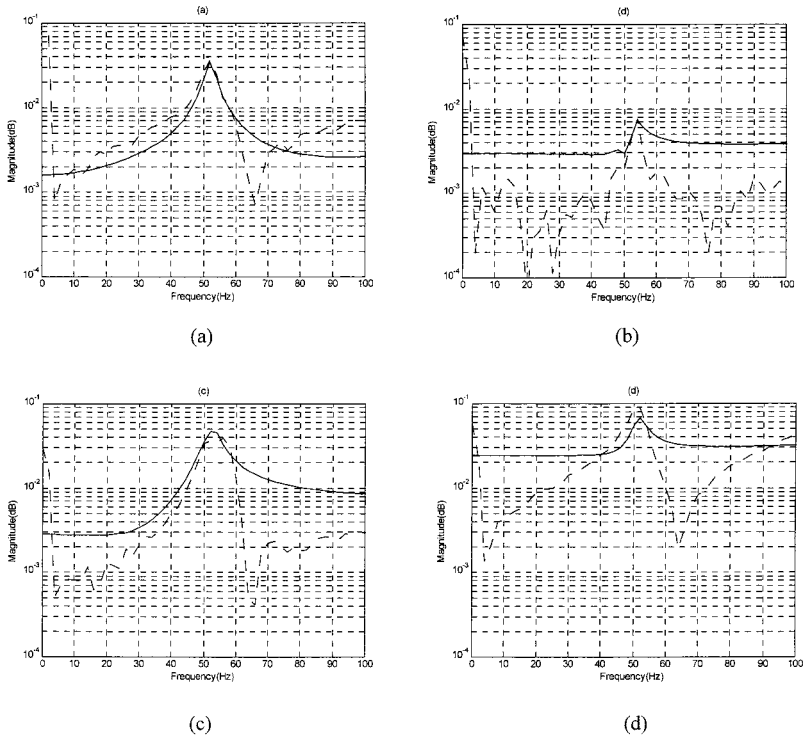

Fig. 8 Frequency response functions of the MIMO system (— — — measured,_regenerated). (*a*) Plant from *Y* actuator to *Y* actuator; (*b*) plant from *Y* actuator to *X* actuator; (*c*) plant from *X* actuator to *Y* actuator; (*d*) plant from *X* actuator to *X* actuator.

$$\hat{\mathbf{S}}(z)=\frac{\mathbf{S}(z)\mathbf{C}(z)}{1+\mathbf{S}(z)\mathbf{C}(z)}. \tag{23}$$

First, we find an LQG feedback controller that stabilizes the open-loop system. The internal model of disturbance can be removed in the design because the performance requirement of the feedback controller is not so stringent as the feedback control. Next, a feedforward controller (FXLMS algorithm with synthetic reference) is introduced to achieve performance without degrading the stability of the feedback-compensated system. This sequential design procedure of hybrid structure has been justified by a separation principle, as detailed in the paper by Clark and Bernstein [14].

Incidentally, the hybrid structure provides yet another advantage over the purely feedforward structure. The impulse response of the feedback-compensated system generally converges faster than the uncompensated one. That is, feedback compensation results in a closed-loop system with larger damping and smaller effective delay. This can be explained by the following argument. An approximate upper bound for the step size in FXLMS algorithm is [19]

$$0<\mu<\frac{2}{P_x(L+2+2\Delta)}, \tag{24}$$

where $P_x=E[x^2(k)]$ is the power of reference signal, L is the length of the weight vector w_{lhi} and Δ is the effective delay of the secondary path. After compensation, the upper bound of the step size is increased due to smaller Δ. Therefore, larger step size can be used so that convergence of FXLMS algorithm is considerably accelerated.

4 Numerical and Experimental Investigations

4.1 Numerical Simulation. Numerical simulation was performed to verify the proposed active control techniques for rotor vibration. The analytical plant model of Eq. (1) was employed in the simulation. The parameters of the rotor are as follows: rotating speed=50 Hz, imbalance mass=5 grams, location of imbalance mass=(30 mm,$4\pi/3$), disc mass=1 Kg, $J_p=0.016\,\mathrm{Kg\cdot m^2}$, $J_i=0.008\,\mathrm{Kg\cdot m^2}$. The sampling rate was selected to be 1 kHz.

In feedback LQG control with internal model, $\mathbf{Q}_c=500\mathbf{I}_{12\times12}$, $\mathbf{R}_c=10\mathbf{I}_{2\times2}$, $\mathbf{Q}_f=300\mathbf{I}_{2\times2}$, $\mathbf{R}_f=50\mathbf{I}_{2\times2}$, and $\zeta_n=1\times10^{-5}$. The result before and after control is activated as shown in Fig. 4, including transient time response and steady-state power spectra of vibration. In feedforward FXLMS with synthetic reference, the step size μ and the weight length were selected to be 0.015 and 10, respectively. The result before and after feedback control is activated as shown in Fig. 5, including transient time response and steady-state power spectra of vibration. In hybrid control (feedback LQG+feedforward FXLMS), $\mathbf{Q}_c=500\mathbf{I}_{12\times12}$, $\mathbf{R}_c=10\mathbf{I}_{2\times2}$, $\mathbf{Q}_f=3\mathbf{I}_{2\times2}$, $\mathbf{R}_f=10\mathbf{I}_{2\times2}$, $\mu=0.15$, and weight length=10. The result before and after feedback control is activated as shown in Fig. 6, including transient time response and steady-state power spectra of vibration. The results of numerical simulation are summarized in Table 1. All of the three methods except the feedback LQG control yield tremendous amount of attenuation. In particular, the hybrid control has the highest convergence speed among all because of the reason mentioned previously.

4.2 Experimental Investigation. In addition to numerical simulation, experiments were carried out to investigate the proposed techniques. A rotor simulator was constructed, as shown in Fig. 7(*a*). The system consists of a 630 gram aluminum disc (6.6 cm in diameter) mounted on a shaft (50 cm in length and 1 cm in diameter) which is driven at the right end by a three-phase, 220 V, two-*hp* induction motor. The speed of the motor can be controlled by using an inverter. There are 16 equally spaced threaded holes drilled on the disc at which one can mount a mass (a 4 gram bolt) to create imbalance. The rotor is supported by two ball bearings. The rotor must be carefully aligned and balanced in advance to

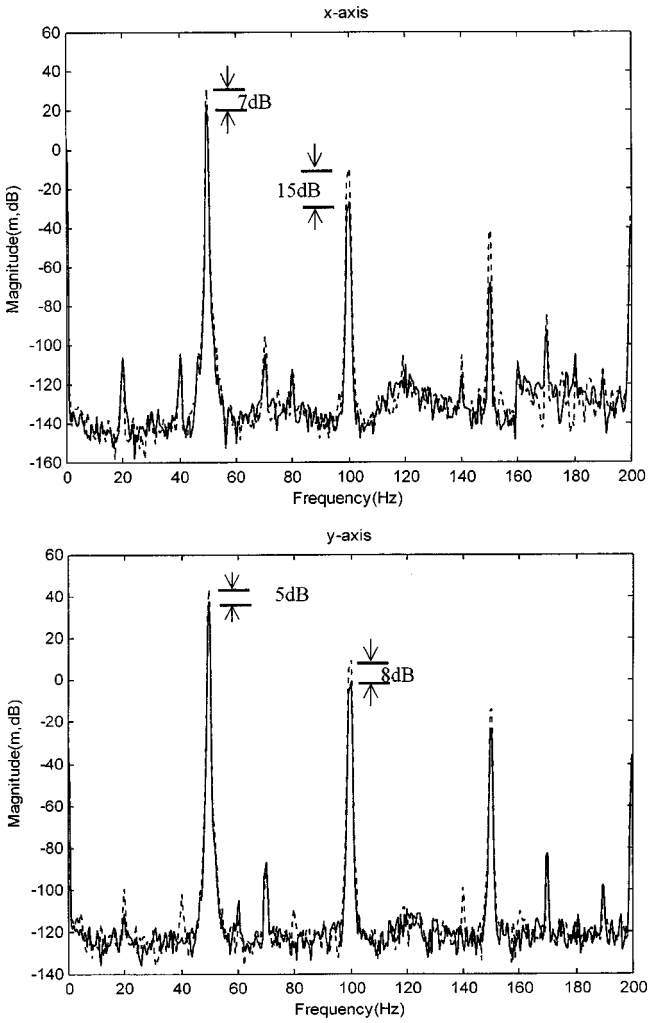

Fig. 9 Experimental results of feedback LQG control. (*a*) *X*-axis power spectra of vibration (. . . control off,_control on); (*b*) *Y*-axis power spectra of vibration (. . . control off,_control on).

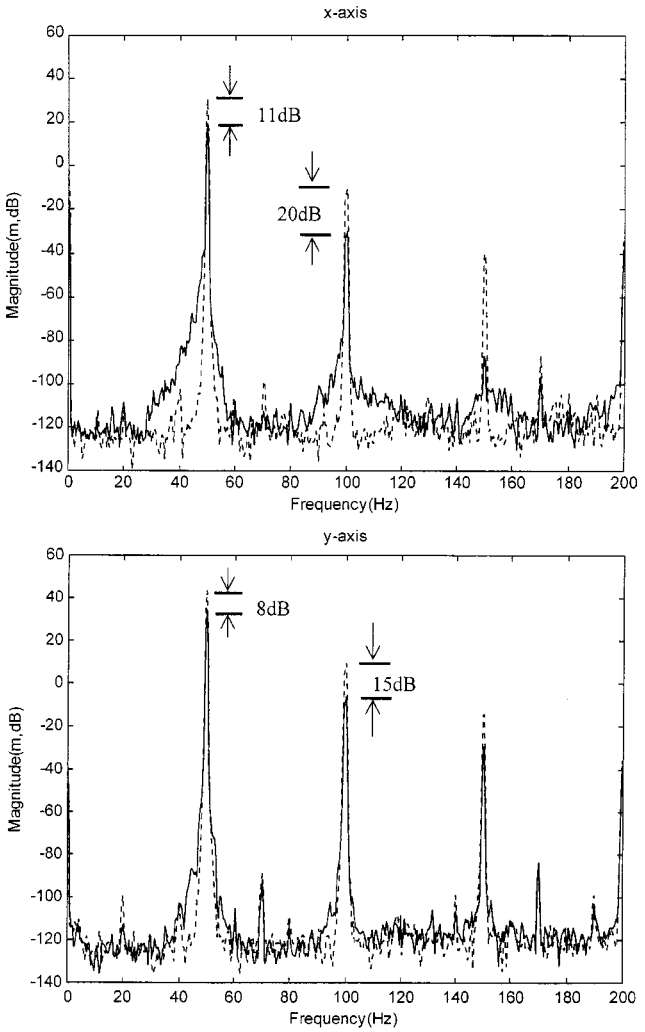

Fig. 10 Experimental results of feedforward FXLMS control with synthetic reference. (*a*) *X*-axis power spectra of vibration (. . . control off,_control on); (*b*) *Y*-axis power spectra of vibration (. . . control off,_control on).

minimize the undesired vibration. Two electro-magnetic actuators are mounted on the horizontal and vertical directions at the left-end bearing housing. A resin column is used at the vertical support to improve mechanical stability and robustness. The details of the mounting mechanisms are shown in Fig. 7(*b*). The actuators are connected to the output of a DSP, TMS320C32. Two eddy current sensors mounted near the disc for measuring the shaft displacements are connected to the input of DSP. The sampling rate is selected to be 4 kHz. A photo switch is used to generate pulses from a reflector on the disc. The rotating speed is then determined by a frequency counting algorithm [18]. This completes a DSP-based active control system for the rotor.

Prior to controller design, the two-input/two-output system model is established by using a experimental frequency-domain identification procedure [20]. The measured and the regenerated frequency response functions of the system are shown in Fig. 8. It can be seen from the frequency response that the plant is more complex than the simple rigid rotor model employed in the numerical simulation. The control is targeted at the fundamental frequency (50 Hz) and the second harmonic (100 Hz), where the modeling error and the higher order dynamics of the plant do not present problems for the narrow-band control. On the basis of the MIMO plant model, controllers are designed by using the aforementioned active control approaches.

In feedback LQG control with internal model, $\mathbf{Q}_c = 100\mathbf{I}_{26\times 26}$, $\mathbf{R}_c = 100\mathbf{I}_{2\times 2}$, $\mathbf{Q}_f = 100\mathbf{I}_{2\times 2}$, $\mathbf{R}_f = \mathbf{I}_{2\times 2}$, and $\zeta_n = 1 \times 10^{-5}$. The result before and after control is activated as shown in Fig. 9. From the figure, 15 dB maximum attenuation is observed. In feedforward FXLMS with synthetic reference, the step size μ and the weight length were selected to be 0.015 and 20, respectively. The rotating speed detected by the photo switch is employed to generate the required synthetic reference. The result before and after feedback control is activated is shown in Fig. 10. From the figure, 20 dB maximum attenuation is observed. The performance is better than the feedback control, although the FXLMS algorithm takes approximately 80 seconds to converge. In hybrid control, $\mathbf{Q}_c = 100\mathbf{I}_{12\times 12}$, $\mathbf{R}_c = 100\mathbf{I}_{2\times 2}$, $\mathbf{Q}_f = 3\mathbf{I}_{2\times 2}$, $\mathbf{R}_f = 10\mathbf{I}_{2\times 2}$, $\mu = 0.15$, and weight length $= 20$. The result before and after feedback control is activated as shown in Fig. 11. From the figure, 25 dB maximum attenuation is observed. The performance is significantly better than the feedback control and the feedforward control. In addition, the FXLMS algorithm takes only 3 seconds to converge. The results of experimental simulation are summarized in Table 2. As expected, the hybrid control indeed incorporating advantages of both feedback control and feedforward control achieved the best performance in terms of vibration attenuation and convergence speed among all methods. The test results demonstrate a capability to decrease vibrations at the sec-

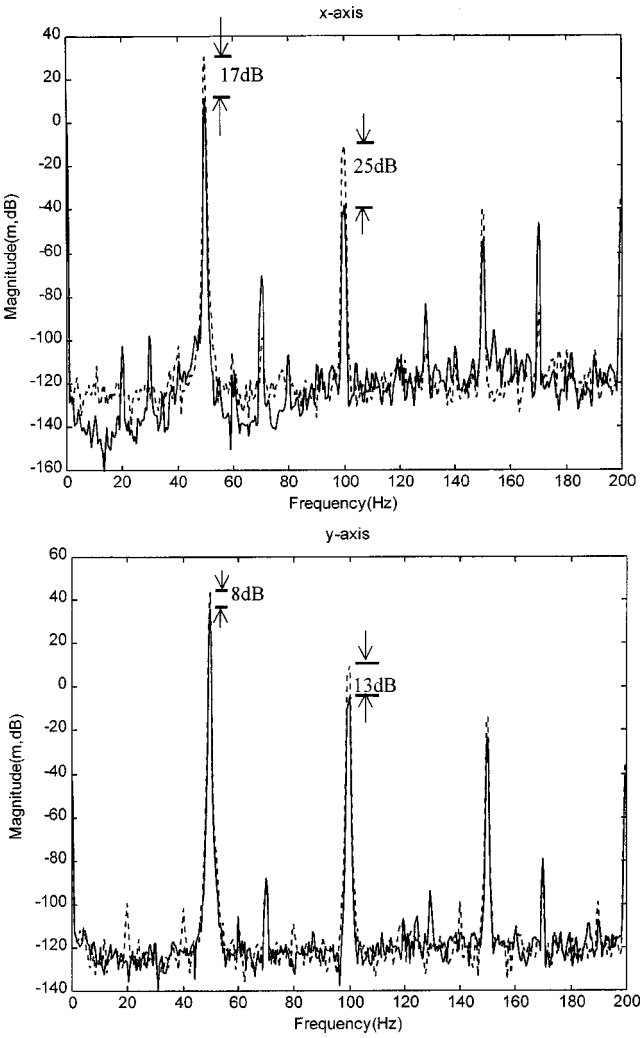

Fig. 11 Experimental results of hybrid control. (*a*) *X*-axis power spectra of vibration (. . . control off,_control on); (*b*) *Y*-axis power spectra of vibration (. . . control off,_control on).

ond and third harmonics. The sources of these harmonics could be misalignment as well as mechanical losseness. The test vibration reductions are significantly less than the simulations. Two reasons that may have contributed to this discrepancy are due to the modeling errors in system identification a 3-sample delay in the DSP board. The degradation of performance is further aggravated when feedforward control is employed. In addition, it can be noted that the noise floor in Figs. 5 and 10 became worse with active control. This is mainly due to the inherent misadjustment problem of the FXLMS algorithm [18].

Table 2 Summary of experimental results

	Axis	Attenuation (dB)		Convergence Speed	Performance
		50 Hz	100 Hz		
Feedback LQG with internal model	x-axis	7	15	Fast	Moderate
	y-axis	5	8		
Feedforward FXLMS	x-axis	11	20	Slow	Good
	y-axis	8	15		
Hybrid FXLMS with LQG	x-axis	17	25	Fast	Very Good
	y-axis	8	13		

5 Conclusions

A DSP-based active control system for suppressing rotor vibration has been developed. Controllers based on feedback structure, feedforward structure and hybrid structure are investigated. Numerical simulation and experimental investigation indicate that the proposed methods are effective in attenuating the periodic disturbances due to common rotor faults. In particular, the hybrid control by using feedback LQG control and feedforward FXLMS algorithm with synthetic reference achieves the best performance in terms of vibration attenuation and convergence speed.

Along the same line of the preliminary results, future research will be focused on the following aspects. The control system should be extended to varying-speed applications. The noise floor became worse with active control due to the inherent misadjustment problem of the FXLMS algorithm. More sophisticated adaptive algorithms should be used to alleviate this problem. The size and weight of the electro-magnetic actuators should be further reduced. The proposed active control system should be tested on the spindle of a practical machine.

Acknowledgments

The work was supported by the Nation Science Council in Taiwan, Republic of China, under the project number NSC 89-2212-E009-007. We would also like to thank Dr. Gary H. Koopmann, Center of Acoustics and Vibration in Penn State University for the motivation of this research topic.

References

[1] Matsumura, F., and Yoshimoto, T., 1986, ''System Modeling and Control Design of a Horizontal Shaft Magnetic Bearing System,'' IEEE Trans. Magn., **MAG-22**, pp. 196–203.
[2] Börvik, P., and Högfors, C., 1986, ''Autobalancing of Rotors,'' J. Sound Vib., **111**, pp. 429–440.
[3] Lum, K.-Y., Coppola, V. T., and Bernstein, D. S., 1996, ''Adaptive Autobalancing Control for an Active Magnetic Bearing Supporting a Rotor with Unknown Mass Imbalance,'' IEEE Trans. Control Syst. Technol., **4**, pp. 587–597.
[4] Lum, K.-Y., Coppola, V. T., and Bernstein, D. S., 1998, ''Adaptive Virtual Autobalancing for a Rigid Rotor with Unknown Mass Imbalance Supported by Magnetic Bearing,'' ASME J. Vibr. Acoust., **120**, pp. 557–570.
[5] Palazzolo, A. B., Lin, R. R., Kascak, A. F., and Alexander, R. M., 1989, ''Active Control of Transient Rotordynamic Vibration by Optimal Control Methods,'' ASME J. Vibr. Acoust., **111**, pp. 264–270.
[6] Palazzolo, A. B., Lin, R. R., Kascak, A. F., Montague, J., and Alexander, R. M., 1991, ''Test and Theory for Piezoelectric Actuator-Active Vibration Control of Rotating Machinery,'' ASME J. Vibr. Acoust., **113**, pp. 167–175.
[7] Palazzolo, A. B., Jagannathan, S., Kascak, A. F., Montague, G. T., and Kiraly, L. J., 1993, ''Hybrid Active Vibration Control of Rotorbearing Systems Using Piezoelectric Actuators,'' ASME J. Vibr. Acoust., **115**, pp. 111–119.
[8] Knospe, C. R., Fedigan, S. J., Hope, R. W., and Williams, R. D., 1997, ''A Multitasking DSP Implementation of Adaptive Magnetic Bearing Control,'' IEEE Trans. Control Syst. Technol., **5**, pp. 230–237.
[9] Bleuler, H., Gähler, C., Herzog, R., Larsonneur, R., Mizuno, T., Siegwart, R., and Woo, S. J., 1994, ''Application of Digital Signal Processors for Industrial Magnetic Bearings,'' IEEE Trans. Control Syst. Technol., **2**, pp. 280–289.
[10] Lalanne, M., and Ferraris G., 1990, *Rotordynamics Prediction in Engineering*, Wiley, New York.
[11] Lund, J. W., and Tonneson, J., 1972, ''Analysis and Experiments in Multiplane Balancing of Flexible Rotors,'' ASME J. Eng. Ind., **94**, p. 233.
[12] Mohamed, A. M., and Busch-Vishniac, I., 1995, ''Imbalance Compensation and Automatic Balancing in Magnetic Bearing System Using the *Q*-parametrization,'' IEEE Trans. Control Syst. Technol., **3**, pp. 202–211.
[13] Morari, M., and Zafirou, E., 1989, *Robust Process Control*, Prentice-Hall, Englewood Cliffs, NJ.
[14] Clark, R. L., and Bernstein, D. S., 1998, ''Hybrid Control: Separation in Design,'' J. Sound Vib., **214**, pp. 784–791.
[15] Lewis, F. L., and Syrmos, V. L., 1995, *Optimal Control*, Wiley, New York.
[16] Lewis, F. L., 1992, *Applied Optimal Control and Estimation*, Prentice-Hall, New York.
[17] Chen, C. T., 1984, *Linear System Theory and Design*, Holt, Rinehart and Winston, New York.
[18] Kuo, S. M., and Morgan, D. R., 1996, *Active Noise Control Systems*, Wiley, New York.
[19] Long, G., Ling, F., and Proakis, J. G., 1992, ''Corrections to 'The LMS algorithm with delayed coefficient adaptation','' IEEE Trans. Signal Process., **40**, pp. 230–232.
[20] Juang, J. N., 1994, *Applied System Identification*, Prentice-Hall, Englewood Cliffs, NJ.